Cell Adhesiveness Serves as a Biophysical Marker for Metastatic Potential

Pranjali Beri[1], Anna Popravko[1], Benjamin Yeoman[1,2], Aditya Kumar[1], Kevin Chen[1], Enio Hodzic[1], Alyssa Chiang[1], Afsheen Banisadr[3], Jesse K. Placone[1], Hannah Carter[4,5], Stephanie I. Fraley[1,4], Parag Katira[2,6], and Adam J. Engler[1,3,7]

ABSTRACT

Tumors are heterogeneous and composed of cells with different dissemination abilities. Despite significant effort, there is no universal biological marker that serves as a metric for metastatic potential of solid tumors. Common to disseminating cells from such tumors, however, is the need to modulate their adhesion as they detach from the tumor and migrate through stroma to intravasate. Adhesion strength is heterogeneous even among cancer cells within a given population, and using a parallel plate flow chamber, we separated and sorted these populations into weakly and strongly adherent groups; when cultured under stromal conditions, this adhesion phenotype was stable over multiple days, sorting cycles, and common across all epithelial tumor lines investigated. Weakly adherent cells displayed increased migration in both two-dimensional and three-dimensional migration assays; this was maintained for several days in culture. Subpopulations did not show differences in expression of proteins involved in the focal adhesion complex but did exhibit intrinsic focal adhesion assembly as well as contractile differences that resulted from differential expression of genes involved in microtubules, cytoskeleton linkages, and motor activity. In human breast tumors, expression of genes associated with the weakly adherent population resulted in worse progression-free and disease-free intervals. These data suggest that adhesion strength could potentially serve as a stable marker for migration and metastatic potential within a given tumor population and that the fraction of weakly adherent cells present within a tumor could act as a physical marker for metastatic potential.

Significance: Cancer cells exhibit heterogeneity in adhesivity, which can be used to predict metastatic potential.

Introduction

The high mortality rate associated with cancer is due to metastasis from a primary tumor to a distal site (1, 2). Patient outcomes typically scale with rate of cell dissemination from the tumor, resulting in lower 5-year survival rates for aggressive tumors such as invasive ductal carcinoma (1). However, determining cell dissemination rate from a tumor is difficult due to heterogeneity, that is cells in the same tumor have different propensities for forming secondary metastases (3–5). Furthermore, there are no universal biochemical markers that predict metastatic potential across solid tumors (4, 6); next-generation assays that use these biomarkers typically only surveil cells post-intravasation.

Biophysical markers, such as cell deformability, are an emerging alternative to assess metastatic potential (7–12). Assays based on these metrics focus largely on characterizing the physical properties of already circulating cells rather than understanding how cancer cells physically interact with and adhere to the extracellular matrix (ECM) at the onset of invasion. Given that all cancer cells must interact with the ECM to initiate metastasis, understanding variations in these interactions can serve as an early indicator of metastatic ability. For optimal cell migration into adjacent parenchyma, cells must turnover their focal adhesions (FA) to move through the tissue effectively; extremely unstable or stable adhesion can arrest migration as the cell can never establish contractile forces or unbind and retract rear portions of the cell (13). Thus, migration speed is a function of the strength of attachment and is maximized when migrating cells can cycle their adhesions (13, 14). Indeed, invasive cancer cells have more dynamic FAs than their noninvasive counterparts (15), and decreased adhesion strength corresponds to increased metastatic potential (16). As a result, the adhesion of cancer cells to ECM proteins is becoming an accepted metric for metastatic potential (17, 18).

Many assays have been developed to demonstrate how adhesion differs in metastatic cells compared with their nonmetastatic counterparts (17, 19–21). However, such assays are either low throughput or not quantitative. It is also difficult to assess adhesive heterogeneity within a single cancer line using these methods (22). We have previously demonstrated that metastatic breast cancer cells display lower cell-ECM adhesion strength than their nonmetastatic counterparts using a spinning-disk shear assay (23, 24), especially when cells are exposed to an environment whose low cation concentration mirrors stroma (25, 26). We also observed an inherent heterogeneity in adhesion strength in multiple lineages including breast, prostate, and lung cancer cell lines (23). Given this information, we developed a parallel plate flow chamber to isolate distinct fractions of cells from a heterogeneous population. Cells were isolated by applying

[1]Department of Bioengineering, University of California, San Diego, La Jolla, California. [2]Department of Mechanical Engineering, San Diego State University, San Diego, California. [3]Biomedical Sciences Program, University of California, San Diego, La Jolla, California. [4]Moores Cancer Center, University of California, San Diego, La Jolla, California. [5]Department of Medicine/Division of Medical Genetics, University of California, San Diego, La Jolla, California. [6]Computational Sciences Research Center, San Diego State University, San Diego, California. [7]Sanford Consortium for Regenerative Medicine, La Jolla, California.

Note: Supplementary data for this article are available at Cancer Research Online (http://cancerres.aacrjournals.org/).

Current affiliation for J.K. Placone: Department of Physics and Engineering, West Chester University, West Chester, Pennsylvania.

Corresponding Author: Adam J. Engler, University of California, San Diego, 9500 Gilman Drive, MC 0695, San Diego, CA 92093. Phone: 858-246-0678; Fax: 858-534-5722; E-mail: aengler@ucsd.edu

Cancer Res 2020;80:901–11

doi: 10.1158/0008-5472.CAN-19-1794

a uniform shear stress to the cell population in the presence of stromal concentrations of Mg and Ca cations (25, 26). Within a given tumor line, we observed significant adhesion heterogeneity and found that the more weakly adherent fraction displays increased migration in both two dimension (2D) and three dimension (3D). This is due to the increased contractility and FA disassembly present in weakly adherent cells, resulting from transcriptomic expression differences in cytoskeletal components. Together, these data suggest that intrinsic differences in adhesion strength of cells within a population can act as markers of intratumoral heterogeneity in metastatic potential and be exploited to biophysically fractionate subpopulations.

Materials and Methods

Cell culture

MDA-MB-231 and MCF7 cells were cultured in DMEM, 10% FBS, and 1% antibiotic/antimycotic; MCF10A and MCF10AT cells were cultured in DMEM/F-12, 5% horse serum, 1% penicillin/streptomycin (Pen/Strep), 0.5 μg/mL hydrocortisone, 20 ng/mL hEGF, 10 μg/mL insulin, 100 ng/mL cholera toxin; NCI-H1299 cells were cultured in RPMI, 10% FBS, and 1% Pen/Strep. Products were purchased from Life Technologies. All cells were obtained from ATCC (authenticated by morphology, growth curve, and isoenzyme analysis), verified *Mycoplasma* free via PCR, and were not used beyond passage 10.

Parallel plate shear assay

Glass plates (Brain Research Laboratories) were sonicated in 70% ethanol and water. Plates were coated with fibronectin at 2 μg/cm^2 for 60 minutes and then blocked with 5% BSA for 2 hours at 37°C. Plates are then seeded with cells at a density of 5,000 cells/cm^2 and incubated overnight. Components of the parallel plate shear assay (polysulfone base plate), 38-μm-thick silicone gasket (SMI), polypropylene luer fixtures (Cole Parmer), 1/8-inch inner diameter tubing (Thermo Fisher Scientific) were assembled and the glass plate was clamped to the base plate containing the inlet and outlet. The inlet tubing was connected to a syringe pump. Shear stress, τ, was calculated using the following equation:

$$\tau = \frac{6\mu Q}{wh^2}, \quad \text{(A)}$$

where μ is viscosity of the fluid, Q is volumetric flow rate, w is the width of the chamber, and h is the height of the chamber.

Isolating weakly and strongly adherent cells

To test adhesion stability of weakly adherent (WA) and strongly adherent (SA) fractions of the population, we first determined an intermediate shear stress to detach roughly 40% of cells (∼170 dynes/cm^2 for MDA-MB-231 cells). PBS without magnesium and calcium and with 4.5 g/L of dextrose was used to shear cells. Cells were subjected to the intermediate shear stress for 3 minutes to isolate WA cells in the flow-through, which was collected at the outlet. 0.25% trypsin-EDTA was added to the device to isolate SA cells. Once cells detached, media was pushed through the device to neutralize the trypsin and remove the SA cells. Both populations were then seeded.

To perform the adhesion stability remixed population assay, WA and SA cells were isolated at day 0, cultured separately for 24 hours, remixed and seeded onto a plate overnight, then re-isolated at 48 hours after the initial isolation.

To isolate the weakest and strongest 2% of the MDA-MB-231 cell population for migration assays, the seeded plate was subjected to a low shear stress (28 dynes/cm^2) for 3 minutes to isolate WA cells in the flow through from the outlet. The shear stress was then increased to a high shear stress (510 dynes/cm^2) for 2 minutes to eliminate intermediate cell fractions. The remaining steps to isolate SA cells are listed above. The weakest MCF10A and MCF10AT cells were isolated using 170 and 130 dynes/cm^2 of shear stress, respectively; the strongest were isolated using 1,275 and 595 dynes/cm^2, respectively.

Coculture assay

MDA-MB-231 and MCF10A cells were trypsinized and resuspended in 25 μmol/L of CellTracker fluorescent probes (Molecular Probes, Life Technologies) in serum-free DMEM: MDA-MB-231 in green CMFDA and MCF10A in Orange CMRA. Cell-dye solutions were incubated at room temperature for 20 minutes. The cells were then centrifuged and resuspended in MDA-MB-231 media. Cells were mixed 50:50 and seeded such that the final seeding density was 5,000 cells/cm^2, then incubated overnight.

Upon isolation of WA and SA cells, both fractions were seeded, incubated overnight, then fixed the following day with 3.7% formaldehyde for 10 minutes. Cells were imaged using a Nikon Eclipse Ti-S microscope at ×10 magnification with FITC and Texas Red and counted by color.

Measuring percent detachment versus metastatic capability

MDA-MB-231, MCF7, MCF10A, and MCF10AT cells were subjected to 250 dynes/cm^2 of shear. The detached and adherent fractions were isolated as described and counted to calculate the fraction of cells detached.

Immunofluorescence staining and FA analysis

Fixed cells were incubated for 10 minutes at room temperature with CellMask Deep Red plasma membrane stain (1:1,000; Thermo Fisher Scientific) in 1 mmol/L $MgCl_2$ solution, followed by incubation for 1 hour at room temperature with blocking solution of 10% goat serum, 0.1% saponin, 1% BSA, 0.03 M glycine in 1 mmol/L $MgCl_2$ solution. Primary paxillin antibody (1:250; ab32084; Abcam) in blocking solution was applied overnight at 4°C. Then, a secondary Alexa Fluor 488-conjugated antibody (1:2,000; Invitrogen) in blocking solution was applied for 1 hour at room temperature, followed by Hoechst 33342 (1:2,000; Invitrogen) in DI water for 10 minutes at room temperature. The cells were subsequently mounted with Fluoromount-G (Southern Biotech). The samples were imaged with a Zeiss LSM 780 confocal microscope (Zeiss) with a 63× oil-immersion objective. A custom-written ImageJ program was used to quantify cell area and FA number and size. All FA metrics were computed across the entire cell to avoid regional biases.

Traction force microscopy

Cell tractions were measured as described and calculated using a custom Matlab routine (27). 2% (v/v) of 0.2 μm diameter 580/605 FluoSpheres microspheres (Invitrogen) were added to the prepolymer solution, composed of 5% acrylamide, 0.06% bisacrylamide, 1% ammonium persulfate (Thermo Fisher Scientific), and 0.1% (v/v) of N,N,N',N'-tetramethylethylenediamine (VWR International). Gels were prepared in 12-well glass bottom plates (Cellvis), which were precleaned in a UV/Ozone cleaner (ProCleaner Plus; Bioforce Nanosciences) and methacrylated to ensure binding of the gel. Collagen was bound to the surface by adding 0.2 mg/mL sulfo-SANPAH and activating with UV light (wavelength 350 nm) for 10 minutes followed by incubation with 0.15 mg/mL type I collagen. Isolated cells were seeded at ∼15,000 cells/cm^2 on the gels and allowed to adhere for 3 hours. Brightfield images were taken of each cell prior to obtaining microsphere displacements at 60×. Bead reference positions were then

reobtained after removing the cells with a 10% (v/v) Triton X solution for 10 minutes. Strain energy was determined from the traction stress map and normalized to cell area.

Western blotting

WA and SA cells were isolated and plated in fibronectin-coated 12-well plates for 3 hours. Cells were lysed with mRIPA supplemented with phosphatase and protease inhibitors as described previously (28). Protein concentration was measured using a BCA assay. Five micrograms of protein was mixed with 50 mmol/L DTT, loading buffer, and mRIPA, heated at 95°C for 5 minutes, and loaded into a Bolt 4% to 12% Bis-Tris Plus gel (Invitrogen) and then run with MES running buffer for 30 minutes at 200 V. Protein was transferred to a nitrocellulose membrane using an iBlot Cell Transfer Stack (Invitrogen). Membrane was blocked with 5% SeaBlock for 1 hour at room temperature then incubated overnight at 4°C with anti-paxillin (Abcam, ab32084), anti-pFAK (Y397; Abcam, ab81298), anti-FAK (Origene, TA506161), anti-actin (Abcam, ab8226), and anti-GAPDH (Abcam, ab8245). The membrane was then incubated for 2 hours at room temperature with Alexa Fluor 680 donkey antimouse (Life Technologies, A32788) and Alexa Fluor 790 donkey anti-rabbit (Life Technologies, A11374) antibodies. The membrane was imaged using a Li-Cor Odyssey CLx and analyzed using Image Studio Lite (Li-Cor).

2D migration assays on collagen gels

2.4 mg/mL type I collagen gels were prepared by mixing collagen (Corning) with PBS, DI water, and 1 M NaOH and adjusted to pH 7.0. Gels were added to a 12-well plates and cured at 37°C for 30 minutes. The weakest and strongest 2% of the cell population were seeded onto the gels and incubated overnight. The cells were imaged with a Nikon Eclipse Ti-S microscope equipped with a temperature- and CO_2-controlled stage. Cells were imaged at 10× in brightfield every 15 minutes for 24 hours. The migration data were analyzed via Fiji. The positions were normalized to the starting point and analyzed via a custom MATLAB script to compute instantaneous speed and cell displacement. Cells that divided or did not remain in the frame for 24 hours were not tracked. Cells that interacted with other cells for more than 2 hours were not tracked, as cell–cell interactions artificially slowed cell speed. For MDA-MB-231 cell migration under drug treatment, cells were treated with either 0.2 μg/mL nocodazole (Cayman Chemical) or 0.5 μg/mL paclitaxel (LC Laboratories). Cells were imaged the following day for 24 hours and tracked as stated above.

2D migration assays on polyacrylamide gels of varying stiffness

Polyacrylamide gels of low and high stiffness were prepared as described in the TFM methods section, without fluorescent microbeads. The high stiffness prepolymer solution has an identical composition to the gels used for TFM, whereas the low stiffness prepolymer solution consists of 3% acrylamide and 0.06% bisacrylamide with all other components identical to the high stiffness gel. Cells were isolated, seeded, and tracked as described previously.

Preparing spheroids of MDA-MB-231 cells

The weakest and strongest 2% of the MDA-MB-231 cell population and unselected cells were isolated and seeded in a 12-well plate overnight. Cells were trypsinized and resuspended in 25 μmol/L CellTracker fluorescent probes (Molecular Probes, Life Technologies) as described above. Cells were then centrifuged and resuspended in a solution of 0.25% Methocult in culture media. A total of 2,500 cells (either WA or SA) were added to wells in a 96-well Corning Ultra-Low Attachment Spheroid Microplate (Corning) then incubated for 48 hours.

3D migration assay in collagen gels

Collagen gels were prepared as described previously. Spheroids were embedded in a collagen gel solution and added to a 24-well plate. Media was added to the top of the gel, and a time 0 image was captured at ×10 magnification with brightfield to obtain initial radius. Embedded spheroids were incubated for 24 hours, after which, they were fixed with 3.7% formaldehyde in solution A for 20 minutes. Spheroids were imaged with a Zeiss LSM 780 confocal microscope at ×10 magnification with the FITC and Texas Red channel. Z-stack images were acquired at 30 μm intervals from the bottom to the top of the spheroid. Maximum intensity projection images were generated and input into a custom Python script to analyze invasive index of spheroid and maximum displacement of cells in the spheroid. Invasive index is defined as:

$$I = \frac{r_{\text{final}}}{r_{\text{initial}}}, \tag{B}$$

where r_{initial} is the radius at time $t = 0$ hours of the spheroid and r_{final} is the radius at time $t = 24$ hours.

RNA sequencing

RNA from WA and SA cells was purified using Qiagen RNeasy Mini Kit (Qiagen, 74104). RNA quality was assessed using TapeStation (Agilent), RNA libraries were prepared using the Illumina TruSeq Stranded RNA, High Throughput Library Prep Kit and sequenced using the Illumina HiSeq 4000 system to generate 50 bp single-end reads. Data were analyzed by Rosalind (https://rosalind.onramp.bio/), with a HyperScale architecture developed by OnRamp BioInformatics, Inc. Reads were trimmed using cutadapt (29). Quality scores were assessed using FastQC (30). Reads were aligned to the Homo sapiens genome build hg19 using STAR (31). Individual sample reads were quantified using HTseq (32) and normalized via relative log expression (RLE) using DESeq2 R library (33). Read Distribution percentages, heatmaps, and sample plots were generated as part of the QC step using RSeQC (34). DEseq2 was also used to calculate fold changes and *P* values. Clustering for the differentially expressed gene heatmap was done using the Partitioning Around Medoids method with the fpc R library (35). Functional enrichment analysis of pathways, gene ontology, domain structure, and other ontologies was performed using HOMER (36). Enrichment was calculated relative to a set of background genes relevant for the experiment.

qPCR

RNA from WA and SA cells was purified using Qiagen RNeasy Mini Kit and reverse transcribed using SuperScript III Reverse Transcriptase (Thermo Fisher Scientific, 18080093). Quantitative PCR was performed (45 cycles, 95°C for 15 seconds followed by 60°C for 1 min) using a 7900HT Fast Real-Time PCR System (Thermo Scientific, 4329001) with the primers listed (Supplementary Table S1), and iQ SYBR Green Supermix (Bio-Rad Laboratories, 1708880). Target genes were normalized to GAPDH and mRNA quantity was calculated on the basis of a standard curve generated from a fibronectin plasmid.

The Cancer Genome Atlas dataset analysis

The Cancer Genome Atlas (TCGA) raw data were downloaded from NIH NCI GDC Data portal directly. Corresponding clinical metadata were obtained from a previous publication (37). Only the patients with breast cancer (BRCA) with reported negative histological

staining for the three markers (Her2, ER, PR) and American Joint Committee on Cancer (AJCC) pathology stages below stage IV were included in our analysis cohort. Patient data were analyzed to determine correlation between gene expression corresponding to WA or SA phenotypes and 5-year survival. Patient data were analyzed by normalizing patient gene expression to z-transformed scores with respect to the differentially expressed genes between the WA and SA subpopulations. The *z*-scores were then summed for every patient, and *z*-score sum-based quantiles were mapped to SA and WA categories based on mean gene expression levels. The Kaplan–Meier method was used to create survival plots comparing the 20% of individuals with the lowest score to the 20% with the highest score. The log-rank test was used to determine significance of survival differences between groups. Survival analyses use the Lifelines python library (https://lifelines.readthedocs.io/en/latest/). Relevant scripts for the analysis of TCGA data are available at: https://github.com/kec162ucsd/Tumor-Heterogeneity-Adhesion-Strength/.

Statistical analysis

2D migration assays, 3D spheroid migration assays, and FA disassembly plots were analyzed using a one-way ANOVA with Tukey test for multiple comparisons. Adhesion stability remixed population assay was analyzed with a two-way ANOVA, with Sidak multiple comparison test. All other comparisons were performed using two-tailed unpaired *t* test unless otherwise indicated. For all analyses, *, $P < 0.05$; **, $P < 0.01$; ***, $P < 0.001$; and ****, $P < 0.0001$. Data expressed as box-and-whisker plots show all points with the whisker ends corresponding to minimum and maximum values. All other values are expressed as mean ± SD. Statistical analyses were performed using Prism software.

Data availability

Data generated in this study was deposited to NCBI under GEO GSE135515. We do not impose any restrictions on data availability.

Results

SA and WA phenotypes are maintained after sort

We fabricated a parallel plate flow chamber that exposes cells to discrete, uniform shear stresses to isolate fractions of cells based on adhesion strength, and study those cells within a heterogeneous population (Supplementary Fig. S1). To ensure that the application of shear did not change the adhesive heterogeneity of the population, we isolated weakly and strongly adherent fractions of MDA-MB-231 cells from a parental cell population by exposing the cell to a shear of 170 dynes/cm^2 and stratifying the populations depending on whether they were found in the flow-through or still attached to the device. After sorting, cells were cultured separately, remixed, seeded into the device, and subsequently sheared. We found no significant changes between the percent of WA and SA cells when tracking cells between days 0 and 2 (**Fig. 1A**), indicating that the parallel plate shear device assesses, but does not alter, the inherent adhesion heterogeneity of the population.

We next wanted to determine if the adhesion phenotype is stably maintained postisolation. We isolated both fractions from MDA-MB-231 cells, cultured them separately in either normal or reduced cation media, and then repeated the isolation on the separated fractions. We found that strongly adherent cells maintained their adherent phenotype 14 days postisolation, regardless of culture conditions. Weakly adherent cells did not maintain their adhesion phenotype in normal culture media as cells reverted back to their distribution in the parental population; if the selection pressure of low stromal-like cation concentrations was maintained postisolation, weakly adherent cells were enriched to more than 70% of the population 6 days postisolation (**Fig. 1B**).

Parallel plate flow chamber can distinguish between WA and SA cell lines

To test the ability of the flow chamber to select for cells known to have a weaker adhesion strength as a result their higher metastatic potential, MDA-MB-231 (metastatic breast cancer line) and MCF10A (nonmalignant breast cell line) cells were seeded in a 50:50 mixture and exposed to a shear stress that should detach the MDA-MB-231 cells but not the MCF10A cells (170 dynes/cm^2 based on population adhesion assays; ref. 23). The fraction of cells that detached contained 41.7% of the total number of MDA-MB-231 cells, whereas only 0.7% of the total number of MCF10A cells were present in the detached fraction (**Fig. 1C**), consistent with 10-fold higher adhesion strength of MCF10A versus MDA-MB-231 cells in the absence of cations (23) and suggesting that this assay could distinguish metastatic cells from noncancerous cells.

To link quantitative adhesiveness to metastatic potential, we exposed four cell lines of varying metastatic potential (high metastatic capability: MDA-MB-231; low metastatic capability: MCF7 and MCF10A; and *H-Ras* transformed: MCF10AT, which give rise to invasive carcinomas *in vivo*; ref. 38) to 250 dynes/cm^2 of shear stress and counted the fraction of detached cells. As expected, cells with greater tumorigenic and/or metastatic potential had significantly greater detachment at the same shear stress in comparison to cells with lower tumorigenic and/or metastatic potential (**Fig. 1D**).

WA cells display greater migratory propensity than SA cells

To assess migration differences in adhesion sorted populations, we isolated the ∼2% most weakly and most strongly adherent cells of the MDA-MB-231 population using 28 and 510 dynes/cm^2, respectively and seeded them onto type I collagen gels. Over 24 hours postplating, we found that WA cells displayed significantly higher average speed than the SA or unselected (nonsheared) cells (**Fig. 2A**). Weakly adherent cells also displayed increased total cell displacement than the SA or unselected cells (**Fig. 2B**; Supplementary Fig. S2). Because the adhesion phenotype appears stable, we investigated if migratory differences were stable. WA and SA cells along with unselected population were imaged after selection, and then re-imaged 2 days later. No significant differences for any population were observed after selection or later while the WA fraction maintained its increased migratory propensity (**Fig. 2C**). The two populations did not exhibit differential proliferation during migration assessments (**Fig. 2D**), suggesting that higher migration speeds for WA cells were not the result of proliferation differences. In addition to sorting a metastatic population, we further demonstrated sorting fidelity by directly comparing the ∼2% most WA and SA of MCF10A and isogenic H-Ras transformed MCF10AT cells. Post-sort on collagen gels, we observed that the WA fraction of MCF10AT cells had increased migration speed and displacement relative to its strongly adherent counterpart, whereas MCF10A cell fractions did not show differences (Supplementary Fig. S3). These data suggest that heterogeneity in migratory phenotype as a result of selection by adhesion strength is only present in more aggressive cells with increased tumorigenic capability.

Migration can often be affected by matrix properties, and so we sought to determine if migration differences are intrinsic and therefore

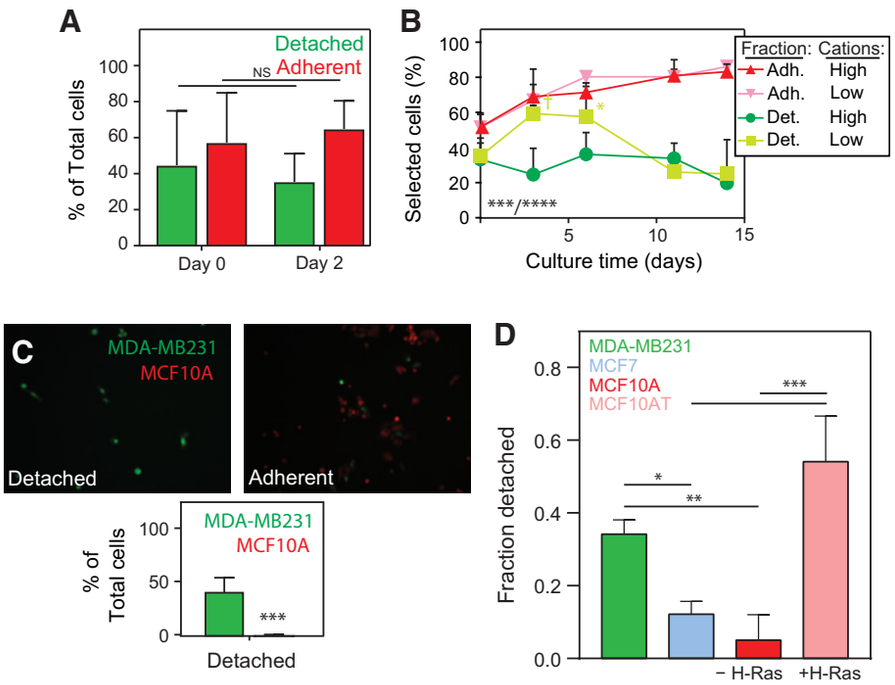

Figure 1.

Low cation PPFC accurately and precisely sorts cancer cell populations that are stable long-term. **A,** MDA-MB-231 populations were sorted at day 0, remixed, and then resorted at day 2. Differences between WA and SA populations were assessed by two-tailed unpaired *t* test ($n = 3$). **B,** Adherent cells post-sort were cultured in high cations for 3, 6, 11, and 14 days and resorted. Cells that detached were cultured in high cations or low cations mirroring stroma prior to resorting. Differences between WA and SA populations as a function of culture time and condition were assessed by two-way ANOVA with Tukey test for multiple comparisons ($n = 3$). For time and condition, ANOVA showed ***, $P < 0.001$ and ****, $P < 0.0001$, respectively as indicated at the corner of the plot. Individual comparisons to their counterpart cation conditions are indicated in the plot with †, $P < 0.1$; *, $P < 0.05$. **C,** Images of cells from the flow-through (detached) and remaining on the plate (adherent) after exposure to shear along with quantification of the percentage of cells that detached relative to plated cells from each line ($n = 3$). ***, $P < 0.001$ for two-tailed unpaired *t* test between lines. **D,** Plot showing the fraction of detached cells from MDA-MB-231, MCF7, and MCF10A and their H-Ras–transformed counterparts MCF10AT after exposure to 250 dynes/cm^2 of shear stress. NS, not significant.

persist regardless of environmental changes that could reduce substrate adhesion. WA and SA MDA-MB-231 cells were plated on polyacrylamide gels of low (300 Pa) and high stiffness (1.8 kPa) and migration observed for 24 hours. WA cells were more migratory that the SA cells independent of substrate stiffness. However, average speed scaled with substrate stiffness gel for both cell fractions, which indicates that both fractions are mechanically sensitive (Supplementary Fig. S4). These results indicate that there are cell intrinsic differences independent of environmental changes that could potentially alter substrate adhesion.

Assays thus far show behaviors in 2D rather than 3D, so we next assessed the outward migration from spheroids containing WA, SA, or unselected cells (**Fig. 2E** and **F**). There was no significant difference in maximum cell displacement (**Fig. 2G**), but the leading edge of weakly adherent cells, that is the distance at which the signal is higher than background (Supplementary Fig. S5), migrated further than SA and unselected cells, indicated by the significantly higher ratio of final radius to initial radius (**Fig. 2F** and **H**). Consistent with 2D migration, these 3D spheroid data bolster the concept that the fraction of tumor cells with the WA most represents those with the highest metastatic potential.

All the cells examined thus far are mammary epithelial, so we next explored whether cells from other epithelial tumors would exhibit the same cation-dependent adhesion sorting and migration phenotype. WA and SA NCI-H1299 metastatic lung cancer cells were isolated and their migration analyzed. As with the metastatic mammary tumor line, WA metastatic lung cancer cells were more migratory than their SA counterparts (Supplementary Fig. S6), suggesting that this behavior may be universal across epithelial tumors.

WA cells have more labile FAs and are more contractile

Migratory differences between WA and SA cells did not result from expression differences in FA proteins, for example pFAK, FAK, paxillin, or actin (**Fig. 3A**). However, we previously found that metastatic cells preferentially disassemble their FAs relative to non-metastatic cells when exposed to low cation conditions (23). Consistent with this, we found that the strongly adherent subpopulation of MDA-MB-231 cells did not fully disassemble FAs after removal of cations. Conversely, WA cells disassembled their FAs in the absence of cations on fibronectin (**Fig. 3B–D**) or on type I collagen-coated substrates (Supplementary Fig. S7). These data suggest that weak adhesion could be driven by differential sensitivity to cations and could therefore enhance migration. Similarly, cancer cells that exhibit increased contractility are also more migratory than their less contractile counterparts (39, 40). To ascertain if adhesive state is coupled with contractility differences, traction force microscopy was performed on cells post-sort. WA cells were significantly more contractile than their strongly adherent counterparts (**Fig. 3E** and **F**), suggesting that weakly adherent cells represent a more aggressive fraction of the population.

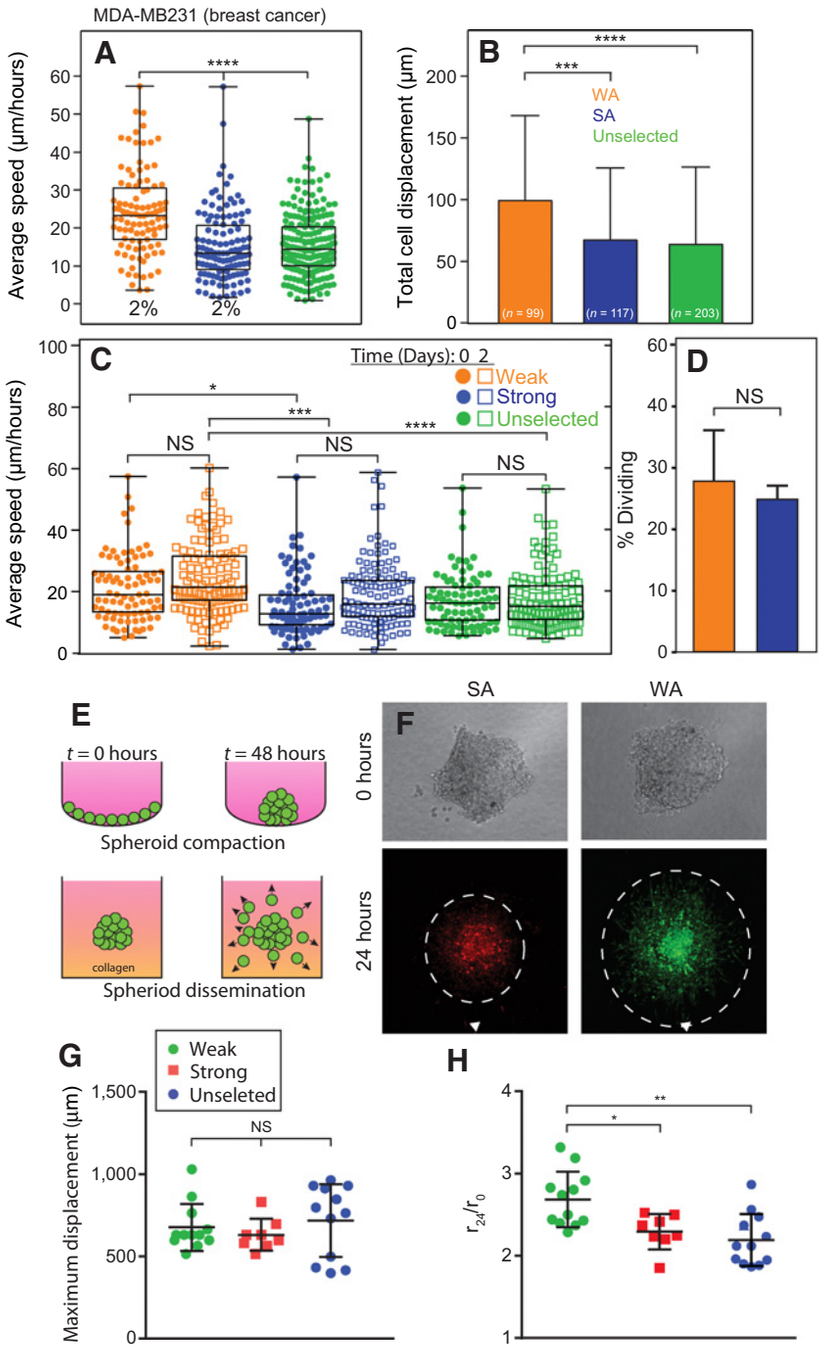

Figure 2.

Sorted populations of single cells and spheroids exhibit and sustain different migration patterns. **A** and **B,** Average speed (**A**) and total displacement (**B**) were plotted for MDA-MB-231 cells sorted by the indicated shear stress and allowed to migrate on collagen gels for 24 hours. Percentages in **A** reflect the portion of each population that detaches or remains adherent at a given stress; $n = 3$ biological replicates for the number of cells per condition inset in the bars in **B**. **C,** Average speed was measured after initial isolation and after 2 days, $n = 3$ biological replicates. **D,** Plot showing the percentage of dividing cells on a collagen gel over 24 hours for cells selected by the indicated shear stress. $n = 3$ biological replicates. **E,** Schematic of tumor spheroid formation (top) and subsequent dissemination (bottom) in a collagen gel. **F,** Brightfield images at the time of spheroid embedding in a collagen gel and fluorescent image 24 hours later. Dashed line, average radius of disseminating cells. **G** and **H,** Plots of maximum (**G**) and normalized (**H**) average outward radial migration of cells selected by indicated shear (see Supplementary Fig. S5, for radius measurements). One-way ANOVA with Tukey test for multiple comparisons was used to indicate significance, where *, $P < 0.05$; **, $P < 0.01$; ***, $P < 0.001$; ***, $P < 0.0001$; NS, not significant.

Intrinsic transcriptional variation in microtubule proteins contributes to increased migration of WA cells

Given that populations sorted at the less restrictive 170 dynes/cm^2 still remain stable with over 1 to 2 weeks in culture, and cells sorted at the more restrictive 28 dynes/cm^2 show cell intrinsic migration differences independent of environmental changes that are stable for days in culture, we next interrogated transcriptional differences underlying WA and SA phenotypes sorted at 28 dynes/cm^2. Stability appears in part because individual populations do not out compete each other, that is cell proliferation rates appear similar (Supplementary Fig. S8). With stable sorting and expansion, we sought to assess differences through post-sort RNA sequencing (RNA-seq). Analyses revealed 500 differentially expressed genes between the subpopulations (**Fig. 4A**); replicates clustered by subpopulation when comparing differentially expressed genes (**Fig. 4B**). Analysis of genes upregulated in weakly adherent cells demonstrated significant enrichment of gene ontology terms involved in microtubule and cytoskeletal organization and binding (**Fig. 4C**). Genes in these categories with the most significant expression differences are involved in cytoskeletal components, specifically microtubule-associated proteins. For example,

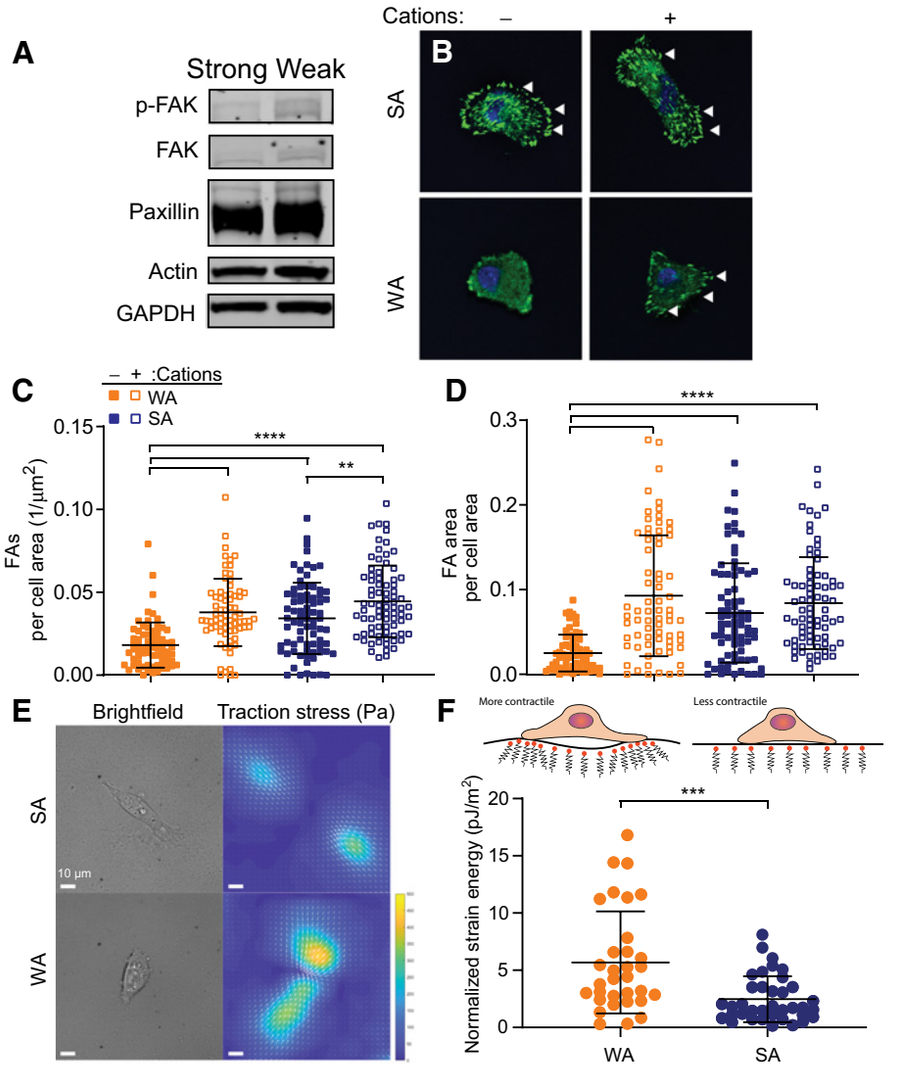

Figure 3.

Adherent phenotypes within a cancer line result from intrinsic adhesion stability and contractility differences. **A,** Comparison of the expression of common FA proteins in SA and WA cells. **B,** Representative images of FAs in SA and WA cells when subjected to with or without cation conditions. **C** and **D,** FA density (**C**) and total area per cell area (**D**) are plotted for the indicated sorting and cation conditions. $n = 3$ biological replicates and >50 cells/condition. One-way ANOVA, with Tukey multiple comparison test was performed for the indicated comparisons with **, $P < 0.01$; ***, $P < 0.001$; ****, $P < 0.0001$. **E,** Brightfield and traction stress plots for cells from the indicated shear conditions. Scale bar, 10 μm. **F,** Plot of normalized strain energy for WA and SA cells. $n = 3$ biological replicates and >30 cells/condition. A two-tailed unpaired t test between lines indicated **, $P < 0.01$; ***, $P < 0.001$; ****, $P < 0.0001$.

GAS2L3 has been implicated in linking microtubules and actin and results in increased FA turnover and migration; SYNE2 is also essential for nuclear-cytoskeletal mechano-transduction in invasion and cell contraction (41–43). Components linking the cytoskeleton to the nuclear or plasma membranes were also implicated, for example AKAP9, which regulates microtubule movement and is highly expressed in highly metastatic cells (**Fig. 4D**; refs. 44, 45). There was also significant enrichment in the expression of motor proteins, specifically those involved in vesicular transport along microtubules (KIF14, DYNC1H1) as well as in cytoskeletal contraction (MYO9A; **Fig. 4C** and **D**). KIF14, in particular, is a potent oncogene that is highly expressed in several cancers, particularly breast cancer, and is linked to improved invasiveness and dynamically changing FAs (46, 47). Changes detected through RNA-seq were validated by qPCR, which confirmed increased expression in WA cells (**Fig. 4E**).

To functionally confirm a link between the upregulated microtubule components in the WA cells and their subsequent increased migration, we exposed both WA and SA cells to either nocodazole or paclitaxel to dissemble or cap microtubules, respectively. When tracking migration, untreated WA cells had increased average speed compared with untreated strongly adherent cells. However when treated with either microtubule-targeting drugs, the WA cells exhibited a significant decrease in average speed, whereas the SA cells were unaffected (**Fig. 4F**). These data suggest that inhibiting the microtubule cytoskeleton preferentially impacts the WA fraction and points to microtubule-affecting agents as potent therapeutic targets.

Finally, we investigated whether differentially expressed genes linked to the highlighted microtubule, cytoskeletal, and microtubule-binding protein ontology terms played a role in human cancer progression. We narrowed the list of genes down to those linked to our highlighted GO terms in **Fig. 4C**, resulting in 100 genes (Supplementary Table S2). Using this gene set, we then analyzed The Cancer Genome Atlas (TCGA) breast cancer dataset and restricted our analysis to patients with triple-negative breast cancer (TNBC) with tumors that ranged from stage I to III. We then compared patients who had gene expression scores that aligned with the SA and WA cells. We observed that patients with gene expression profiles similar to the WA cells had decreased progression-free intervals (**Fig. 5A**) and disease-free intervals (**Fig. 5B**) compared with patients with gene expression profiles similar to the SA cells. These data suggest that increased expression of genes associated with microtubule and microtubule-binding proteins, as present in the WA fraction, could define an

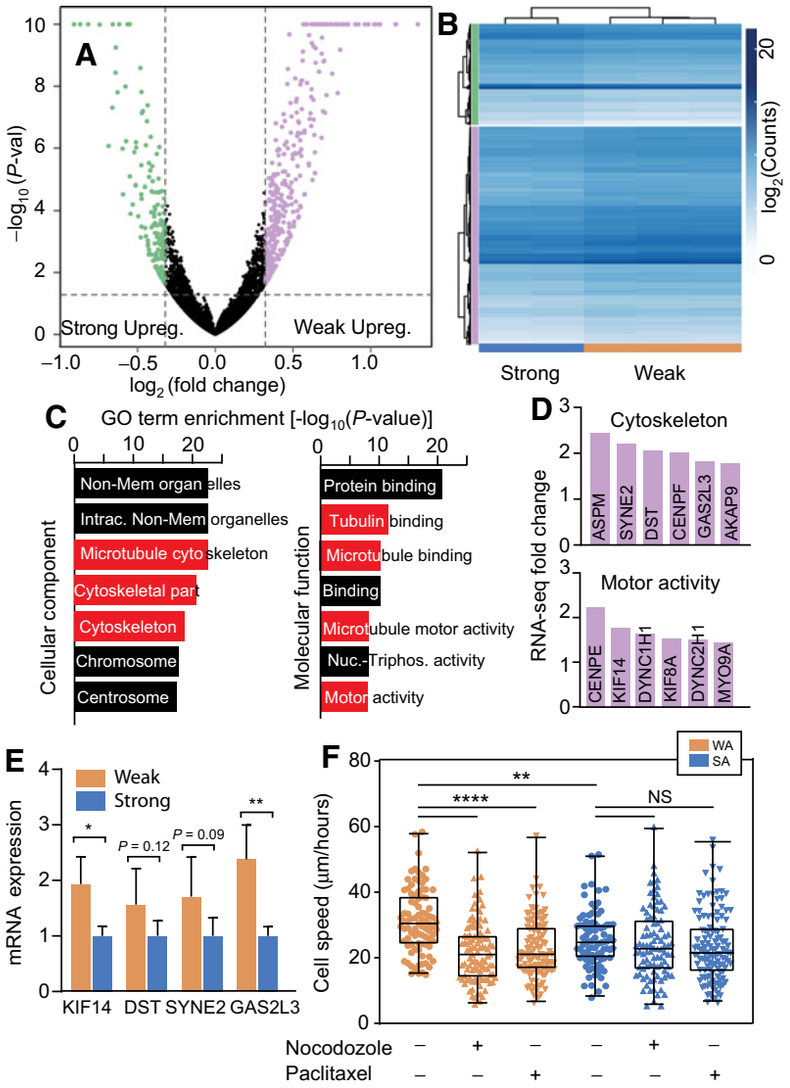

Figure 4.

RNA-seq identifies intrinsic patterns that indicate structural rather than expression changes in adhesion. **A,** Differences in gene expression between WA and SA MDA-MB-231 cells. **B,** Hierarchical clustering of differentially expressed genes between WA and SA cells. Vertical bars indicate clustering of genes that are upregulated in SA cells and WA cells. **C,** Gene ontology terms that are upregulated in the WA subpopulation. Cytoskeletal and microtubule gene ontology terms, as well as proteins that bind to these components, were significantly upregulated in WA cells. **D,** Expressions of genes upregulated in cytoskeleton and motor activity, normalized to SA subpopulation. **E,** Validation of RNA-seq gene expression differences via qPCR for select genes. *, $P < 0.05$ and **, $P < 0.01$ for two-tailed unpaired t test between WA and SA cells. **F,** Average speed of WA and SA cells when treated with microtubule-targeting drugs. At identical concentrations of nocodazole (0.2 μg/mL) and paclitaxel (0.5 μg/mL), WA cells displayed a significant decrease in migration speed, whereas the SA cells demonstrated no change. One-way ANOVA with Tukey multiple comparison test was performed for the indicated comparisons with **, $P < 0.01$; ***, $P < 0.001$; and ****, $P < 0.0001$. NS, not significant.

"adhesive signature" that results in an increase in metastatic potential and promotes human breast tumor progression.

Discussion

Because of the highly heterogeneous nature of tumor cells, both within a given tumor as well as across tumors from different patients, it is difficult to assess tumor aggressiveness and the likelihood of metastasis. In addition, there are no universal biochemical markers that can be utilized to determine metastatic potential. The emergence of biophysical markers is a new approach to identifying the most aggressive subpopulations of the tumor population. Common cell–ECM interactions of early dissemination of cancer cells of different tumor origins and subsequent ECM deformation reflect the importance of identifying biophysical markers as metrics for metastatic potential (1, 2). To accomplish this, we utilized a parallel plate flow chamber to study the correlation between decreased adhesion strength of cells to ECM proteins and their subsequent metastatic potential. In conjunction with our previous studies (23), we showed that metastatic cancer cells are significantly less adherent than their nonmetastatic counterparts. This is demonstrated by the ability to select for MDA-MB-231 cells over MCF10A cells from a mixed population. We also found that WA can serve as a potential marker for metastatic potential, which was demonstrated by the greater percent detachments of MDA-MB-231 and MCF10AT cells in comparison to MCF7 and MCF10A cells at the same shear stress.

This study also identified heterogeneity in adhesion strength of cells within a metastatic cancer cell population, especially under stromal-like cation conditions, which may be linked to heterogeneity in metastatic potential of cells within a tumor population and/or circulating tumor cells. This notion is supported by our observations that WA MDA-MB-231 cells exhibited increased migration in comparison to their strongly adherent counterparts. These differences in migration exist in both 2D and 3D environments, which indicates that the WA subpopulation represents the cells that are more likely to leave the primary tumor and establish secondary metastases (48–50). The stability of this increased migratory propensity for multiple days post-sorting further demonstrates the intrinsic nature of this phenotype. In addition, recapitulating this phenotype in metastatic lung cancer cells suggests that adhesion

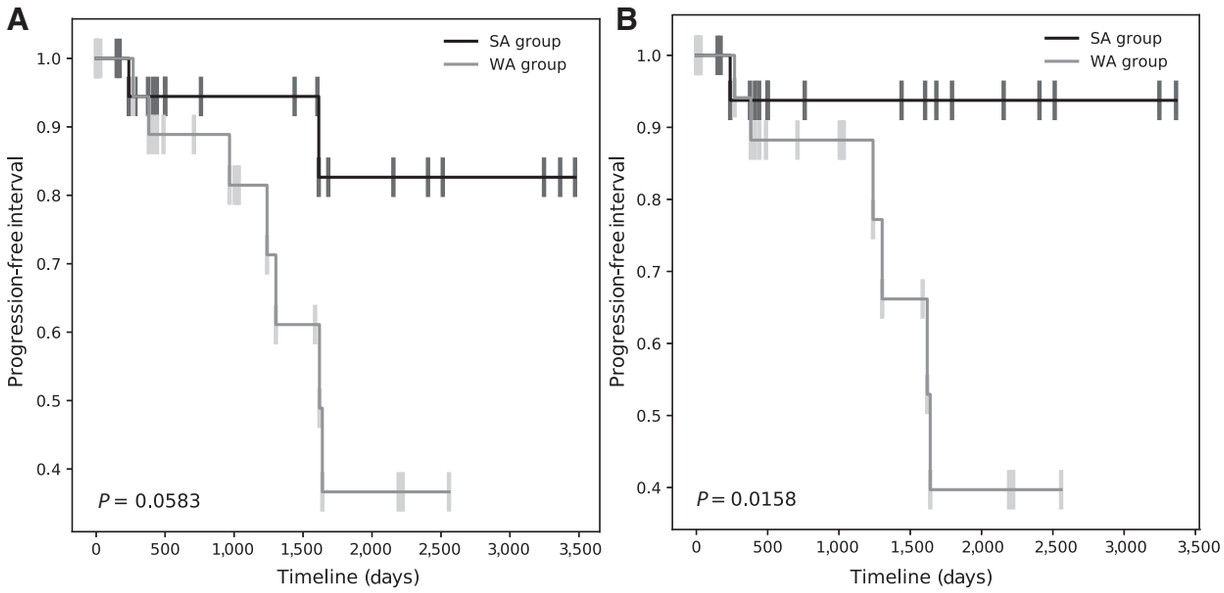

Figure 5.

Expression of microtubule-associated genes resembling WA fraction predicts poor outcome in patients with breast cancer. **A** and **B,** Progression-free interval (**A**) and disease-free interval (**B**) of patients with TNBC with stage I to III tumors. Patients with gene expression that resembled SA and WA cells were compared. Genes were restricted to those associated with highlighted gene ontology terms in **Fig. 4C**, resulting in a cohort of 100 genes.

strength is broadly involved in the more migratory subpopulations within tumors from multiple epithelial backgrounds.

The ability to select this more migratory subpopulation of the cell line stems from differences in FA disassembly between the WA and SA cells. Faster FA disassembly of WA cells is consistent with previous findings that link quicker FA disassembly to more migratory cell lines (15, 51, 52). In addition, WA cells are more contractile than their SA counterparts, where increased contractility has also been linked to increased migration and more aggressive cancers (39, 40). Differences in migration, FA assembly, and contractility can be tied to inherent transcriptomic differences between WA and SA cells; genes linked to the cytoskeleton, specifically to microtubules, as well as motor proteins involved in vesicular transport and contraction showed significant differential expression. When we compared human patients with breast cancer with gene expression signatures that resembled the WA and SA cells for our genes of interest, we observed decreased progression-free and disease-free intervals, implying that tumors resembling the WA fraction are more aggressive. Several standard cancer therapy drugs (nocodazole, taxols, etc.) target microtubules to reduce the growth and spread of aggressive tumors, indicating that differences in microtubules and the cytoskeleton could explain the heterogeneity of tumor cell populations. We confirmed these findings by treating WA cells to nocodazole and paclitaxel and found that their migration speed reduced to that of the SA cells, whose speed was unaffected by both drugs. Therefore, targeting the cytoskeleton is potentially an important method of restricting the motility of highly aggressive subpopulations early in tumor development and suppressing the migratory populations that we observe (53).

This study reveals a strategy to identify distinct subpopulations via shear separation that can be implemented to study the dissemination of cells from a variety of epithelial cancers. Comparing WA cell populations across multiple metastatic cell lines of various tumor origins could enable the identification of similarities among the most aggressive subpopulation in an effort to identify more universal targeted treatments. Finally, this shear assay can be adapted to study diseases with a similar adhesion component, highlighting the versatility of this technique.

Disclosure of Potential Conflicts of Interest

S.I. Fraley has ownership interest (including patents) in Melio Lab, Inc., and is an unpaid consultant/advisory board relationship member for Melio Labs, Inc. No potential conflicts of interest were disclosed by the other authors.

Authors' Contributions

Conception and design: P. Beri, A. Banisadr, A.J. Engler
Development of methodology: P. Beri, B. Yeoman, A.J. Engler
Acquisition of data (provided animals, acquired and managed patients, provided facilities, etc.): P. Beri, A. Popravko, B. Yeoman, A. Kumar, K. Chen, E. Hodzic, A. Chiang, J.K. Placone
Analysis and interpretation of data (e.g., statistical analysis, biostatistics, computational analysis): P. Beri, B. Yeoman, K. Chen, H. Carter, S.I. Fraley, P. Katira, A.J. Engler
Writing, review, and/or revision of the manuscript: P. Beri, S.I. Fraley, A.J. Engler
Administrative, technical, or material support (i.e., reporting or organizing data, constructing databases): A.J. Engler

Acknowledgments

The authors thank Drs. Jing Yang and Eugene Yeo (UCSD) as well as Cian O'Leary (RSCI) for helpful discussions and the UCSD Campus Research Machine Shop for assistance in device fabrication. The results shown here are in part based upon data generated by the TCGA Research Network: https://www.cancer.gov/tcga. A.J. Engler acknowledges grant support from the NIH (R01CA206880 and R21CA217735) and National Science Foundation (1763139). P. Katira acknowledges grant support from the National Science Foundation (1763132) and the Army Research Office (W911NF-17-1-0413). S.I. Fraley acknowledges grant support from the Faculty Early Career

Development Program (CAREER) Awards (1651855) and American Cancer Society Institutional Research Grant (15-172-45-IRG) provided through the Moores Cancer Center at the University of California San Diego. P. Beri, A. Banisadr, and A. Kumar were supported by the National Science Foundation GRFP. NIH fellowship awards also supported A. Kumar (T32AR060712) and J.K. Placone (F32HL126406) as well as the ARCS/Roche Foundation Scholar Award Program in the Life Science (to A. Kumar).

The costs of publication of this article were defrayed in part by the payment of page charges. This article must therefore be hereby marked *advertisement* in accordance with 18 U.S.C. Section 1734 solely to indicate this fact.

Received June 7, 2019; revised September 30, 2019; accepted December 16, 2019; published first December 19, 2019.

References

1. Steeg PS. Targeting metastasis. Nat Rev Cancer 2016;16:201–18.
2. Siegel RL, Miller KD, Jemal A. Cancer statistics, 2018. CA Cancer J Clin 2018;68:7–30.
3. Quintana E, Shackleton M, Sabel MS, Fullen DR, Johnson TM, Morrison SJ. Efficient tumour formation by single human melanoma cells. Nature 2008;456:593.
4. Polyak K. Heterogeneity in breast cancer. J Clin Invest 2011;121:3786–8.
5. Sun X-x, Yu Q. Intra-tumor heterogeneity of cancer cells and its implications for cancer treatment. Acta Pharmacol Sin 2015;36:1219.
6. Liu Y, Nenutil R, Appleyard MV, Murray K, Boylan M, Thompson AM, et al. Lack of correlation of stem cell markers in breast cancer stem cells. Br J Cancer 2014;110:2063.
7. Alibert C, Goud B, Manneville JB. Are cancer cells really softer than normal cells? Biol Cell 2017;109:167–89.
8. Dudani JS, Gossett DR, Tse HTK, Di Carlo D. Pinched-flow hydrodynamic stretching of single-cells. Lab Chip 2013;13:3728–34.
9. Gossett DR, Tse HTK, Lee SA, Ying Y, Lindgren AG, Yang OO, et al. Hydrodynamic stretching of single cells for large population mechanical phenotyping. Proc Natl Acad Sci 2012;109:7630–5.
10. Qi DP, Gill NK, Santiskulvong C, Sifuentes J, Dorigo O, Rao J, et al. Screening cell mechanotype by parallel microfiltration. Sci Rep 2015;5:17595.
11. Nyberg KD, Scott MB, Bruce SL, Gopinath AB, Bikos D, Mason TG, et al. The physical origins of transit time measurements for rapid, single cell mechanotyping. Lab Chip 2016;16:3330–9.
12. Beri P, Matte BF, Fattet L, Kim D, Yang J, Engler AJ. Biomaterials to model and measure epithelial cancers. Nat Rev Mater 2018;3:418–30.
13. Ridley AJ, Schwartz MA, Burridge K, Firtel RA, Ginsberg MH, Borisy G, et al. Cell migration: integrating signals from front to back. Science 2003;302:1704–9.
14. DiMilla P, Stone J, Quinn J, Albelda S, Lauffenburger D. Maximal migration of human smooth muscle cells on fibronectin and type IV collagen occurs at an intermediate attachment strength. J Cell Biol 1993;122:729–37.
15. Bijian K, Lougheed C, Su J, Xu B, Yu H, Wu JH, et al. Targeting focal adhesion turnover in invasive breast cancer cells by the purine derivative reversine. Br J Cancer 2013;109:2810–8.
16. Indra I, Undyala V, Kandow C, Thirumurthi U, Dembo M, Beningo KA. An *in vitro* correlation of mechanical forces and metastatic capacity. Phys Biol 2011;8:015015.
17. Reticker-Flynn NE, Malta DF, Winslow MM, Lamar JM, Xu MJ, Underhill GH, et al. A combinatorial extracellular matrix platform identifies cell-extracellular matrix interactions that correlate with metastasis. Nat Commun 2012;3:1122.
18. Yates CM, McGettrick HM, Nash GB, Rainger GE. In: Dwek M, Schumacher U, Brooks SA, editors.Metastasis research protocols. New York, NY, Springer New York; 2014. p. 57–75.
19. Palmer CP, Mycielska ME, Burcu H, Osman K, Collins T, Beckerman R, et al. Single cell adhesion measuring apparatus (SCAMA): application to cancer cell lines of different metastatic potential and voltage-gated Na+ channel expression. Eur Biophys J 2008;37:359–68.
20. Garcia AJ, Gallant ND. Stick and grip. Cell Biochem Biophys 2003;39:61–73.
21. Veiseh M, Kwon DH, Borowsky AD, Tolg C, Leong HS, Lewis JD, et al. Cellular heterogeneity profiling by hyaluronan probes reveals an invasive but slow-growing breast tumor subset. Proc Natl Acad Sci 2014;111:E1731–9.
22. Gupta PB, Fillmore CM, Jiang G, Shapira SD, Tao K, Kuperwasser C, et al. Stochastic state transitions give rise to phenotypic equilibrium in populations of cancer cells. Cell 2011;146:633–44.
23. Fuhrmann A, Banisadr A, Beri P, Tlsty TD, Engler AJ. Metastatic state of cancer cells may be indicated by adhesion strength. Biophys J 2017;112:736–45.
24. Fuhrmann A, Li J, Chien S, Engler AJ. Cation type specific cell remodeling regulates attachment strength. PLoS One 2014;9:e102424.
25. Seltzer MH, Rosato FE, Fletcher MJ. Serum and tissue magnesium levels in human breast carcinoma. J Surg Res 1970;10:159–62.
26. Seltzer MH, Rosato FE, Fletcher MJ. Serum and tissue calcium in human breast carcinoma. Cancer Res 1970;30:615–6.
27. Lo Sardo V, Chubukov P, Ferguson W, Kumar A, Teng EL, Duran M, et al. Unveiling the role of the most impactful cardiovascular risk locus through haplotype editing. Cell 2018;175:1796–810.
28. Kumar A, Thomas SK, Wong KC, Sardo VL, Cheah DS, Hou Y-H, et al. Mechanical activation of noncoding-RNA-mediated regulation of disease-associated phenotypes in human cardiomyocytes. Nat Biomed Eng 2019;3:137–46.
29. Martin M. Cutadapt removes adapter sequences from high-throughput sequencing reads. EMBnet J 2011;17:3.
30. Andrews S. FAST QC: A quality control tool for high throughput sequence data. http://www.bioinformatics.babraham.ac.uk/projects/fastqc/.
31. Dobin A, Davis CA, Schlesinger F, Drenkow J, Zaleski C, Jha S, et al. STAR: ultrafast universal RNA-seq aligner. Bioinformatics 2012;29:15–21.
32. Anders S, Pyl PT, Huber W. HTSeq—a Python framework to work with high-throughput sequencing data. Bioinformatics 2014;31:166–9.
33. Love MI, Huber W, Anders S. Moderated estimation of fold change and dispersion for RNA-seq data with DESeq2. Genome Biol 2014;15:550.
34. Wang L, Wang S, Li W. RSeQC: quality control of RNA-seq experiments. Bioinformatics 2012;28:2184–5.
35. Hennig C. Cran-package fpc. http://cran.r-project.org/web/packages/fpc/
36. Heinz S, Benner C, Spann N, Bertolino E, Lin YC, Laslo P, et al. Simple combinations of lineage-determining transcription factors prime cis-regulatory elements required for macrophage and B cell identities. Mol Cell 2010;38:576–89.
37. Liu J, Lichtenberg T, Hoadley KA, Poisson LM, Lazar AJ, Cherniack AD, et al. An Integrated TCGA pan-cancer clinical data resource to drive high-quality survival outcome analytics. Cell 2018;173:400–16.
38. Heppner GH, Wolman SR. MCF-10AT: a model for human breast cancer development. Breast J 1999;5:122–9.
39. Mierke CT, Kollmannsberger P, Zitterbart DP, Diez G, Koch TM, Marg S, et al. Vinculin facilitates cell invasion into three-dimensional collagen matrices. J Biol Chem 2010;285:13121–30.
40. Kraning-Rush CM, Califano JP, Reinhart-King CA. Cellular traction stresses increase with increasing metastatic potential. PLoS One 2012;7:e32572.
41. Stroud MJ, Kammerer RA, Ballestrem C. Characterization of G2L3 (GAS2-like 3), a new microtubule- and actin-binding protein related to spectraplakins. J Biol Chem 2011;286:24987–95.
42. Friedl P, Wolf K, Lammerding J. Nuclear mechanics during cell migration. Curr Opin Cell Biol 2011;23:55–64.
43. Jayo A, Malboubi M, Antoku S, Chang W, Ortiz-Zapater E, Groen C, et al. Fascin regulates nuclear movement and deformation in migrating cells. Dev Cell 2016;38:371–83.
44. Kumar N, Gupta S, Dabral S, Singh S, Sehrawat S. Role of exchange protein directly activated by cAMP (EPAC1) in breast cancer cell migration and apoptosis. Mol Cell Biochem 2017;430:115–25.
45. Yang M-H, Hu ZY, Xu C, Xie LY, Wang XY, Chen SY, et al. MALAT1 promotes colorectal cancer cell proliferation/migration/invasion via PRKA kinase anchor protein 9. Biochim Biophys Acta 2015;1852:166–74.
46. Ahmed SM, Thériault BL, Uppalapati M, Chiu CWN, Gallie BL, Sidhu SS, et al. KIF14 negatively regulates Rap1a–Radil signaling during breast cancer progression. J Cell Biol 2012;199:951–67.
47. Thériault BL, Basavarajappa HD, Lim H, Pajovic S, Gallie BL, Corson TW. Transcriptional and epigenetic regulation of KIF14 overexpression in ovarian cancer. PLoS One 2014;9:e91540.
48. Mi L, Zhu F, Yang X, Lu J, Zheng Y, Zhao Q, et al. The metastatic suppressor NDRG1 inhibits EMT, migration and invasion through interaction and

promotion of caveolin-1 ubiquitylation in human colorectal cancer cells. Oncogene 2017;36:4323.
49. Hu J, Verkman AS. Increased migration and metastatic potential of tumor cells expressing aquaporin water channels. FASEB J 2006;20:1892–4.
50. Slack JK, Adams RB, Rovin JD, Bissonette EA, Stoker CE, Parsons JT. Alterations in the focal adhesion kinase/Src signal transduction pathway correlate with increased migratory capacity of prostate carcinoma cells. Oncogene 2001;20:1152.
51. Frame MC, Fincham VJ, Carragher NO, Wyke JA. v-SRC'S hold over actin and cell adhesions. Nat Rev Mol Cell Biol 2002;3:233.
52. McLean GW, Carragher NO, Avizienyte E, Evans J, Brunton VG, Frame MC. The role of focal-adhesion kinase in cancer—a new therapeutic opportunity. Nat Rev Cancer 2005;5:505.
53. Feng R, Li S, Lu C, Andreas C, Stolz DB, Mapara MY, et al. Targeting the microtubular network as a new antimyeloma strategy. Mol Cancer Ther 2011;10:1886–96.